POWER ELECTRONICS AND DRIVES
Vol. 1(36), No. 2, 2016 DOI: 10.5277/PED160204

ANTI-WINDUP STRATEGY FOR AN LQ CURRENT CONTROLLER WITH OSCILLATORY TERMS FOR THREE-PHASE GRID-TIE VSCs IN SMES SYSTEMS*

ANDRZEJ GAŁECKI, LECH GRZESIAK, BARŁOMIEJ UFNALSKI,
ARKADIUSZ KASZEWSKI, MAREK MICHALCZUK

Warsaw University of Technology, Institute of Control and Industrial Electronics,
Electrical Drive Division, ul. Koszykowa 75, 00-662 Warszawa, Poland,
phone: +48 (22) 234 60 25, e-mail: andrzej.galecki@pw.edu.pl

Abstract: The paper presents a linear-quadratic current controller with damped oscillatory terms designed for three-phase grid-tie voltage source converters used in SMES systems and operated under distorted grid voltage conditions. Special emphasis is placed on a synthesis of an anti-windup mechanism to prevent wind-up derived from the oscillatory terms by the use of a new active damping loop based on a simple moving average method. As a consequence, the current feedback gain may be increased without unwanted overshoot and overruns, and performance of the system can be improved.

Keywords: *grid-connected converter, linear-quadratic control, resonant control, current control, anti-windup*

1. INTRODUCTION

Large-scale grid-connected energy storage, which is capable of supporting smooth supply on the grid is going to tip the balance of propagating the distributed generation systems (DGS) including renewable sources. Compressed air energy storage [1], Li-ion batteries [2], flywheels [3] and superconducting magnetic energy storage (SMES) [4] are among the leaders in the field of modern solutions. An integral part of these systems are specialized power converters with digital signal controllers whose architecture has been developed for executing power converter control algorithms. In this paper, selected issues of the current control of grid-tie voltage source converter (VSC) operating under distorted grid voltage conditions

* Manuscript received: October 25, 2016; accepted: December 14, 2016.

are considered with respect to the software developed for the physical 250 kVA SMES systems (currently under construction).

Various current control strategies for grid-connected VSCs operating under distorted grid voltage conditions have been proposed [5]–[9]. In order to ensure the rejection of sinusoidal disturbances caused by grid voltage imbalance and distortion caused by higher harmonics, selected oscillatory terms are readily used [10], [11] also with frequency adaptation ability [12] for the DGS. During converter operation, the control system with oscillatory terms can produce a control signal, which is not feasible without performance deterioration due to the plant input limitations. This windup problem [13] can lead to unsafe operation.

Two main strategies to face the windup problem in the power converter control with oscillatory terms (also referred to as resonant controllers) have been introduced in the literature. The first idea is based on control damping of the resonator in second-order generalized integrator (SOGI). It was presented in a voltage source inverter at the stage of conception [14]. Next, it is adopted to current limiting strategies during fault ridethrough of inverters [15] and used in a double-feed induction generator rotor-side converter control in $\alpha\beta$ coordinate, even after temporary voltage rotor limitation [16]. In the latter application, damping is controlled independently for each resonant path, where multiple gain coefficients and multiple low-pass filters are required. The second strategy is to implement saturation in the resonant terms based on reduced-order generalized integrator (ROGI) [17]. The three-phase current controller with oscillatory terms implemented in stationary frames with the use of a ROGI approach is more efficient than the SOGI because ROGI requires half the states than SOGI to be implemented. However, if the current controller with the same harmonic compensation capability is realized in the rotating reference frame (RRF), the same number of states is necessary [18].

In this paper, the anti-windup mechanism is developed for the linear-quadratic (LQ) current control with oscillatory terms designed for the three-phase grid-tie converter. The grid-side VSC control is coordinated in the RRF, where damped oscillatory terms based on SOGI structure are used. Therefore, the concept based on control damping in resonant terms has been adopted. A newly developed active damping mechanism based on simple moving average (SMA) [19] method is proposed. The performance of the control system in transient and steady-state has been verified in the simulation study.

The SMES coil can be connected to the grid by a variety of power electronic converter topologies. One of the more popular ones is based on cascade connection of grid-tie VSC and DC/DC converter referred to as the VSC-based SMES in the literature [4] and conceptually shown in Fig. 1. In this case, the three-level neutral-point-clamped (NPC) [20] grid-connected VSC is equipped with an LC filter on the grid side. An overview of the design of LC and LCL filters is given in [21] and is out of the scope of this paper.

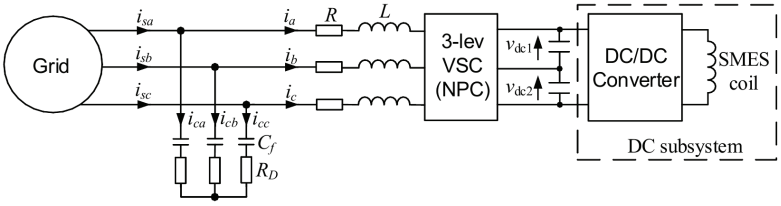

Fig. 1. Block diagram of the SMES system connected to the grid via VSC

The DC/DC converter with SMES coil part is referred to as DC subsystem and its requirements are given in Section 2. An essential part of this paper associated with the LQ current control with damped oscillatory terms designed for grid-tie VSC is discussed in Section 3, while the numerical results are presented in Section 4.

2. DC SUBSYSTEM

The SMES is an electrical device used for storing energy in the magnetic field associated with a circulating current flowing through a superconducting coil. Due to circulating current SMES unit can deliver energy with well-nigh instantaneous response. The maximum available power of the unit depends on the voltage of the intermediate DC-link v_{dc} and the current of the coil i_{coil} as follows: $p_{\text{SMES}}^{\max} = v_{dc} i_{\text{coil}}$.

The two-quadrant DC/DC chopper is an interface between the VSC and the coil [22], [23]. The topology of the DC/DC converter is presented in Fig. 2. The SMES has to be constructed in such a way as to ensure closed path for the coil current. For practical reasons, the coil operates with unidirectional current.

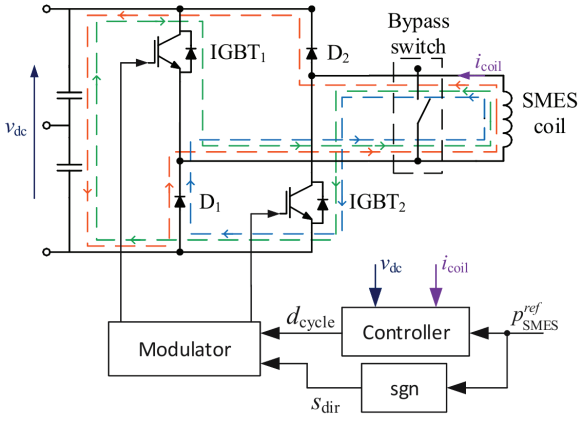

Fig. 2. The topology and control of DC/DC chopper

The chopper consists of two branches of series connected IGBT transistor and diode. This topology ensures the closed path of the coil current for every state of IGBT switches. If both IGBTs are in blocking state, the SMES is discharged through diodes D_1, D_2 (red line in Fig. 2). If both IGBTs conduct the energy from the DC-link capacitors and charges the SMES (green line in Fig. 2). If one of IGBTs conducts the current circulating through the IGBT and diode and no energy is exchanged between the SMES and the intermediate DC-link (blue line in Fig. 2). In the case of standby mode the additional bypass is used, which is more effective than closing the current path through the diode and the transistor. Additionally, the bypass switch allows disconnecting the chopper for the maintenance operations.

The chopper operates at 2.5 kHz switching frequency. The output power of the SMES is controlled by changing the duty cycle of the IGBT gate signals d_{cycle}. The SMES discharge/charge mode is selected based on the sign of the required output power.

3. CONTROL SYSTEM OF THE GRID-CONNECTED VSC

The proposed control system of the grid-connected VSC is presented in Fig. 3 taking into account several assumptions.

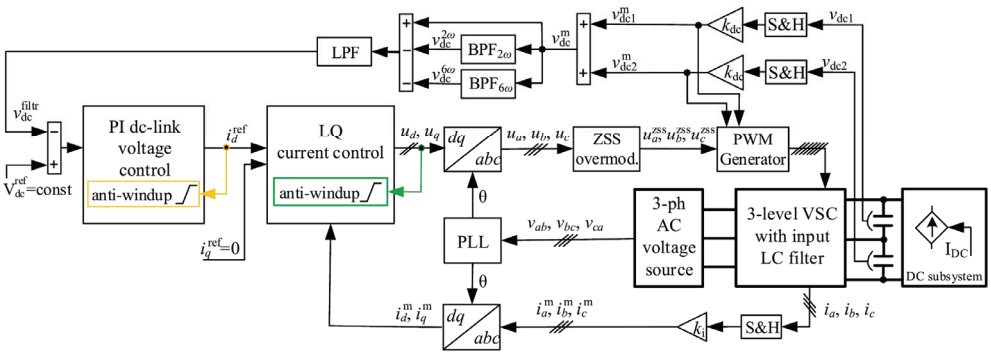

Fig. 3. Block diagram of the grid-connected VSC control

It should be noted that in physical models the SMES system is typically connected to the grid through a transformer. For the purposes of focus on VSC current control numerical study it has been modeled as a three phase voltage source, where the 3% unbalance and selected odd harmonics (5th – 6%, 7th – 5%, 11th – 3.0%, 13th – 2.0%, where THD_u = 8.0%) are included. Moreover, in the numerical model the DC subsystem consists of two-quadrant DC/DC converter and SMES coil is modeled as a controlled current source on account of the fact that only selected issues of grid-side converter control have been discussed. It is also assumed that input

filter capacitor currents $i_{ca} \ll i_a$, $i_{cb} \ll i_b$, $i_{cc} \ll i_c$ and their components in the grid currents are not compensated. Selected parameters of the numerical model are given in Table 1.

In the inner loop, the LQ current controller with damped oscillatory terms is applied. The control structure is designed in a positive-sequence RRF with a power grid angular frequency ω [24], where amplitude preservation-based Park transformation is used. In the proportional-integral path, the classical anti-windup implementation is realized based on integral clamping [25]. The current control system is equipped with oscillatory terms. They enable the grid-side converter to obtain a balanced and nearly sinusoidal shape of the input currents.

Table 1. Selected parameters of the numerical model

Symbol	Value	Description
V_{dc}	700 V	Nominal DC-link voltage
V	400 V	Nominal grid phase-to-phase voltage RMS value
ω	100 πs^{-1}	Nominal angular frequency of the grid voltage
L_s	0.1 mH	Inductances of the grid
R_s	0.01 Ω	Resistances of the grid
L	0.12 mH	Inductances of the input filter choke
R	0.04 Ω	Resistances of the input filter choke
C_f	0.12 mF	Capacitances of the input filter capacitors
R_D	0.5 Ω	Damping resistances of the input filter
I_{DC}	358 A	Nominal DC subsystem current
C	6.0 mF	Capacitance of the DC-link capacitor
F_s	4 kHz	Switching frequency
TH-ZSS-PWM	Continuous	Modulation type
T_s	1/Fs	Sampling time
k_{dc}	1/350	DC-link voltage scaling factor
k_i	1/600	Current scaling factor

In the outer loop, a PI-type DC-link voltage controller with an anti-windup based on integrator clamping is used. For the outer loop controller design, the closed inner-current loop transfer function between the input signal i_d^{ref} and the output signal i_q^{ref} is calculated using MATLAB®. Then it is approximated by a first-order lag element. Finally, the DC-link voltage controller is tuned using the Naslin polynomial approach [26]. The details of PI-type DC-link voltage controller design are presented in our previous work [27]. In order to extract the 2ω and 6ω components of the DC-link voltage measuring signal v_{dc}^m, two band-pass filters ($\text{BPF}_{2\omega}$, $\text{BPF}_{6\omega}$) are used. Then the obtained components $v_{dc}^{2\omega}, v_{dc}^{6\omega}$ are subtracted from v_{dc}^m. In practice, first order low-pass filter (LPF) is also needed to suppress high-frequency harmonic components caused by DC/DC converter switching transients and measurement noise.

In order to track the grid voltage fundamental component vector angle θ a phase-locked loop (PLL) based on two band-pass filters and delayed signal cancellation method [28] is used. In order to ensure a maximum linear range and almost optimal current harmonics a pulse-width modulation with triplen harmonic zero-sequence signal (THZSS-PWM) is used. The control signals $u_a^{zss}, u_b^{zss}, u_c^{zss}$ should be between –1 and 1 due to the appointed PWM generator based on two triangular carriers covering the area from the –1 to 1. Therefore, the u_d and u_q control signals amplitudes are located up to $U_{\max} = 2/\sqrt{3} \cong 1.1547$.

3.1. LQ CURRENT CONTROLLER WITH DAMPED OSCILLATORY TERMS

The current control structure with oscillatory terms is presented in Fig. 4, where **K_p**, **K_I**, **K_{r2}**, **K_{r6}**, **K_{r12}** are matrices of the state-feedback control gains in the proportional, integral and oscillatory paths, respectively.

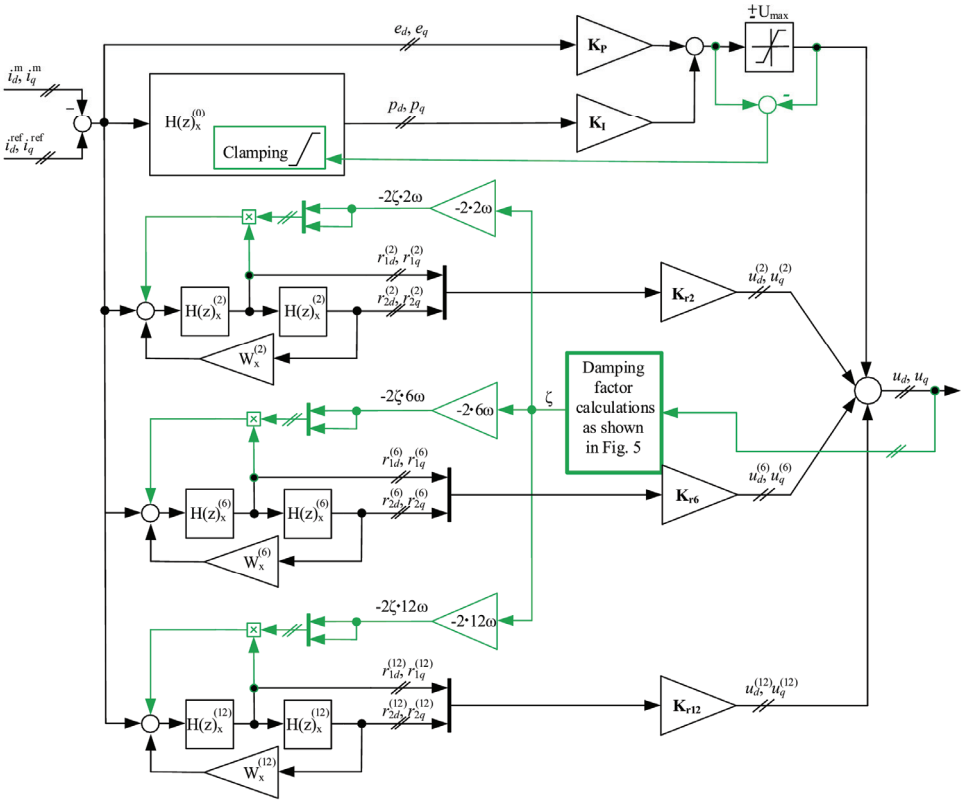

Fig. 4. Block diagram of LQ current control with oscillatory terms and anti-windup mechanism

The proportional current control of grid-connected VSC does not provide zero steady-state tracking errors $e_d = i_d^{\text{ref}} - i_d^m$ and $e_q = i_q^{\text{ref}} - i_q^m$ for step type reference commands. Thus, the current control is extended by integral terms trough the introduction of the two new variables p_d and p_q in accordance with

$$\frac{d}{dt} p_x = e_x , \tag{1}$$

where subscript $x = \{d, q\}$.

Similarly, in order to minimize the sinusoidal component of the error in the current tracking caused by the voltage distortion, the oscillatory terms are incorporated. Each of the 5th, 7th, 11th and 13th higher harmonics of the grid voltage (in natural reference frame) usually has the largest amplitudes than harmonics above the 13th. In the *dq* reference frame, the voltage imbalance causes to appear as 2ω oscillations while the 5th and 7th harmonics in *abc* become 6ω oscillations and the 11th and 13th harmonics are visible as 12ω oscillations. Therefore, six oscillatory terms are incorporated into the current control structure in parallel to the proportional and integral paths. They can be described by the following differential equations

$$\frac{d}{dt} r_{1x}^{(h)} = r_{2x}^{(h)} , \tag{2a}$$

$$\frac{d}{dt} r_{2x}^{(h)} = e_x - (h\omega)^2 r_{1x}^{(h)} - 2\zeta(h\omega) r_{2x}^{(h)} , \tag{2b}$$

where subscript $x = \{d, q\}$, $h = \{2, 6, 12\}$ is a selected harmonic order, ζ is a damping factor assumed at the same level for all oscillatory terms. In order to convert the oscillatory terms from the continuous-time to the discrete-time domain, a Tustin approximation with pre-warping is used, where

$$H(z)_x^{(h)} = \frac{1}{s}\bigg|_{s=\frac{h\omega}{\tan\left(\frac{h\omega T_s}{2}\right)}\frac{z-1}{z+1}} = \frac{\tan\left(\frac{h\omega T_s}{2}\right)}{h\omega}\frac{z+1}{z-1} , \tag{3}$$

and

$$W_x^{(h)} = -(h\omega)^2 , \tag{4}$$

for $h = \{2, 6, 12\}$, while

$$H(z)_x^{(0)} = \frac{1}{s}\bigg|_{s=\frac{2}{T_s}\frac{z-1}{z+1}} = \frac{T_s}{2}\frac{z+1}{z-1} , \tag{5}$$

where subscript $x = \{d, q\}$.

Moreover, current controller designed according to the states-space approach could have differed methods of introducing the reference input [29]. On the one hand, the response to the reference signals i_d^{ref} and i_q^{ref} can be driven only by the integral and oscillatory paths of the current controller. In this case, the feed-forward paths from the reference currents are not present. The $\mathbf{K_p}$ part of the current controller is driven by state signals [30]. On the other hand, the feed-forward paths from reference currents can be incorporated. One of the possible methods for determining the gains value in this feed-forward path is to take them the same as in the $\mathbf{K_p}$ matrix. In this case, $\mathbf{K_p}$ part of the current controller can be driven by tracking error signals e_d and e_q as it is stated in [31]. The LQ current controller with integral terms with a different introduction of the reference input has been compared and commented in our previous work [32].

3.2. DETERMINATION OF DAMPING FACTOR FOR OSCILLATORY TERMS

The block diagram of damping factor calculations is presented in Fig. 5.

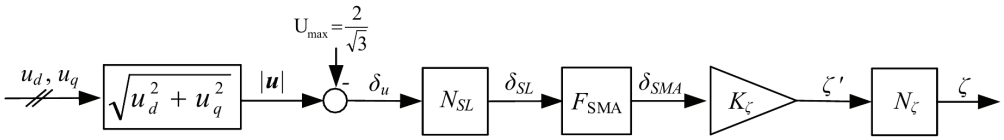

Fig. 5. Block diagram of damping factor calculations

At the beginning, $|\boldsymbol{u}|$ is calculated in terms of coordinates given by u_d, u_q. For the sensitivity level $\delta_u^{\min} = 0$, active damping mechanism is activated if the module of control vector exceeds the $U_{\max}$ limit.

$$\delta_{SL} = N_{SL}(\delta_u) = \begin{cases} \delta_u, & \text{if} \quad \delta_u \geq \delta_u^{\min}, \\ \delta_u^{\min}, & \text{if} \quad \delta_u < \delta_u^{\min}. \end{cases} \tag{6}$$

Then, the δ_{SL} signal is smoothed using F_{SMA} filter based on SMA method to avoid violent fluctuations in the oscillatory terms. This is accomplished using the following formula

$$\delta_{SMA}(n) = F_{SMA}(\delta_{SL}(n)) = \frac{1}{M+1}\sum_{k=0}^{M} x(n-k), \tag{7}$$

where $M = T_{\text{aver}}/T_s$ is a number of past samples while T_{aver} is an averaging period.

It is proposed here to set $T_{\text{aver}} = 0.02$ s because such a period corresponds to six peaks of 50 Hz component of the control signal waveform in *abc* coordinates. In order to damp resonant term efficiently fast the gain K_ζ is used as follows

$$\zeta' = K_\zeta \delta_{SMA} . \tag{8}$$

Moreover, it is important to keep damping factor ζ in the rigid limits. On the one hand, in the positive minimum $\zeta_{\min} = 0$. On the other hand, in the maximum $\zeta_{\max} = 1$ to suppress no more than the border, where the oscillations disappear and term becomes inertial. Finally, the damping factor ζ is defined as

$$\zeta = N_\zeta(\zeta') = \begin{cases} \zeta_{\max}, & \text{if} \quad \zeta' > \zeta_{\max}, \\ \zeta', & \text{if} \quad \zeta_{\min} \le \zeta' \le \zeta_{\max}, , \\ \zeta_{\min}, & \text{if} \quad \zeta' < \zeta_{\min}. \end{cases} \tag{9}$$

The response time of the active control damping loop strongly depends on selecting the K_ζ gain which was designed by trial-and-error method.

The following method of the K_ζ gain selection has been introduced. It is initialized when the LQ current controller and the DC-link voltage controller are already designed. In this paper, for the purpose of the K_ζ adjusting, the appropriate simulation scenario in the numerical model was prepared by taking into account step variation of nominal load and 75% voltage dip in one of the phases. The K_ζ gain is selected in an iterative process. In the first iteration, $K_\zeta = 0$ has been set, which implies $\zeta = 0$. In succeeding iterations, a positive value of K_ζ has been gradually increased by trial-and-error method until $|\mathbf{u}|$ it reaches a prior set threshold 105% of $U_{\max}$. In the ideal case the threshold for $|\mathbf{u}|$ is 100% of $U_{\max}$, but the 5% precision level has been assumed taking into account specific conditions like a sampling time and an accuracy of numerical calculations. The selected K_ζ value has been retained for the final simulation study some of the results of which are presented in Section 5.

3.3. STATE-SPACE MODEL FOR CURRENT CONTROLLER DESIGN

For the purposes of the current controller design, the linear state-space model (1) is obtained using a small-signal modeling technique [30]. The linearization problem is simplified assuming that v_{dc} is V_{dc} = const and ω = const. Accordingly, the state-space model in the *dq* rotating reference frame is presented as follows

$$\frac{d}{dt}\mathbf{x} = \mathbf{A}\mathbf{x} + \mathbf{B}\mathbf{u} , \tag{10a}$$

where

$$\mathbf{A}=\begin{bmatrix}-\dfrac{R}{L} & \omega\\ -\omega & -\dfrac{R}{L}\end{bmatrix},\quad \mathbf{x}=\begin{bmatrix}i_d^m\\ i_q^m\end{bmatrix},\quad \mathbf{B}=\begin{bmatrix}-\dfrac{v_{dc}}{L}k_i & 0\\ 0 & -\dfrac{v_{dc}}{L}k_i\end{bmatrix},\quad \mathbf{u}=\begin{bmatrix}u_d\\ u_q\end{bmatrix}, \tag{10b}$$

There are two state signals i_d^m and i_q^m collected in the state vector **x** and two control signals u_d and u_q collected in the control vector **u**. There are also two matrices: **A** – the state matrix and **B** – the control matrix. The disturbance matrix and the associated disturbance vector containing the grid voltages are omitted, because no feed-forward paths from disturbances are considered here.

The state-space model with a state vector augmented by the auxiliary state variables collected in the **p** vector (integral part) and the state variables collected in the **r** vector (oscillatory terms) is given by

$$\frac{d}{dt}\mathbf{x}_{\text{aug}}=\mathbf{A}_{\text{aug}}\mathbf{x}_{\text{aug}}+\mathbf{B}_{\text{aug}}\mathbf{u}\,, \tag{11a}$$

where

$$\mathbf{A}_{\text{aug}}=\begin{bmatrix}\mathbf{A_0} & \mathbf{0_{2\times2}} & \mathbf{0_{2\times2}} & \mathbf{0_{2\times2}}\\ \mathbf{A_I} & \mathbf{A_{(2)}} & \mathbf{0_{2\times2}} & \mathbf{0_{2\times2}}\\ \mathbf{A_I} & \mathbf{0_{2\times2}} & \mathbf{A_{(6)}} & \mathbf{0_{2\times2}}\\ \mathbf{A_I} & \mathbf{0_{2\times2}} & \mathbf{0_{2\times2}} & \mathbf{A_{(12)}}\end{bmatrix},\quad \mathbf{x}_{\text{aug}}=\begin{bmatrix}\mathbf{x}\\ \mathbf{p}\\ \mathbf{r}\end{bmatrix},\quad \mathbf{B}_{\text{aug}}=\begin{bmatrix}\mathbf{B}\\ \mathbf{0}\end{bmatrix},\quad \mathbf{u}=\begin{bmatrix}u_d\\ u_q\end{bmatrix}, \tag{11b}$$

given that

$$\mathbf{A_0}=\begin{bmatrix}\mathbf{A} & \mathbf{0_{2\times2}}\\ \mathbf{I_{2\times2}} & \mathbf{0_{2\times2}}\end{bmatrix},\quad \mathbf{A_I}=\begin{bmatrix}\mathbf{0_{2\times2}} & \mathbf{0_{2\times2}}\\ \mathbf{I_{2\times2}} & \mathbf{0_{2\times2}}\end{bmatrix},\quad \mathbf{A_{(h)}}=\begin{bmatrix}\mathbf{0_{2\times2}} & \mathbf{I_{2\times2}}\\ \mathbf{W_{(h)}} & \mathbf{0_{2\times2}}\end{bmatrix}, \tag{11c}$$

and where $\mathbf{W_{(h)}}=-\text{diag}([(h\omega)^2,(h\omega)^2])$ for $h=\{2,6,12\}$.

Therefore, the augmented state matrix $\mathbf{A}_{\text{aug}}$, the augmented control matrix $\mathbf{B}_{\text{aug}}$ and the new augmented state vector $\mathbf{x}_{\text{aug}}$, where: $\mathbf{p}=[p_d,p_q]^T$, $\mathbf{r}=[r_{(2)},r_{(6)},r_{(12)}]^T$ and where $\mathbf{r}_{(h)}=[r_{1d}^{(h)},r_{1q}^{(h)},r_{2d}^{(h)},r_{2q}^{(h)},]^T$ for h = {2, 6, 12} are defined.

3.4. LQ CURRENT CONTROLLER DESIGN

The full-state feedback current controller has been designed using the augmented state-space model given in Section 3.3. In order to calculate the current controller gains collected in the matrix $\mathbf{K}_{\text{aug}}$ = [$\mathbf{K_p}$, $\mathbf{K_I}$, $\mathbf{K_{r2}}$, $\mathbf{K_{r6}}$, $\mathbf{K_{r12}}$], the LQ method is cho-

sen. The *lqrd* MATLAB's function is used, where the state-feedback law $\mathbf{u}(k) = -\mathbf{K}_{\text{aug}}\mathbf{x}_{\text{aug}}(k)$ minimizes a discrete cost function equivalent to the continuous cost function

$$J = \int_0^{\infty} (\mathbf{x}_{\text{aug}}^T \mathbf{Q}_{\text{aug}} \mathbf{x}_{\text{aug}} + \mathbf{u}^T \mathbf{R}\mathbf{u})\, dt\,, \tag{12}$$

where $\mathbf{Q}_{\text{aug}} = \text{diag}([\mathbf{Q}, \mathbf{Q}_{\text{p}}, \mathbf{Q}_{\text{r}}])$ and $\mathbf{R}$ are weighting matrices. It was assumed that the same penalty weight is applied in both axes d and q of the current control structure. Accordingly, weighting matrices are presented as follows: $\mathbf{R} = \text{diag}([\text{r}, \text{r}])$, $\mathbf{Q} = \text{diag}([q,\ q])$, $\mathbf{Q}_p = \text{diag}([q_p,\ q_p])$ and $\mathbf{Q}_r = \text{diag}(\mathbf{Q}_{(2)},\ \mathbf{Q}_{(6)},\ \mathbf{Q}_{(12)})$ and where $\mathbf{Q}_{(h)} = \text{diag}\left(\left[q_r^{(h)}, q_r^{(h)}, \frac{q_r^{(h)}}{(2\omega)^2}, \frac{q_r^{(h)}}{(2\omega)^2} \right]\right)$ for $h = \{2, 6, 12\}$.

In the next step, the penalty weights are selected by trial-and-error method. It has been shown that selecting weighting factors for the LQR procedure can be reduced to finding powers with the selected common base [33].

4. NUMERICAL RESULTS

The control system allows bidirectional energy flow between grid and DC subsystem of SMES. The dynamic behavior of the grid-converter VSC operated under unbalanced and distorted grid voltage conditions is summarized for comparison in Fig. 6 to Fig. 8. The energy flow from the grid to the DC subsystem takes place between 0.2 s and 0.3 s, while from 0.35 s to 0.45 s the direction is opposite. The behavior of the system under selected voltage dip (voltage drop in phase A down to 60 V RMS) is shown for comparison, in Fig. 9 and in Fig. 10, where from 0.2 s to 0.4 s the energy flow from the grid to the DC subsystem is tested. From the converter control point of view, the three current control cases are verified in a simulation study.

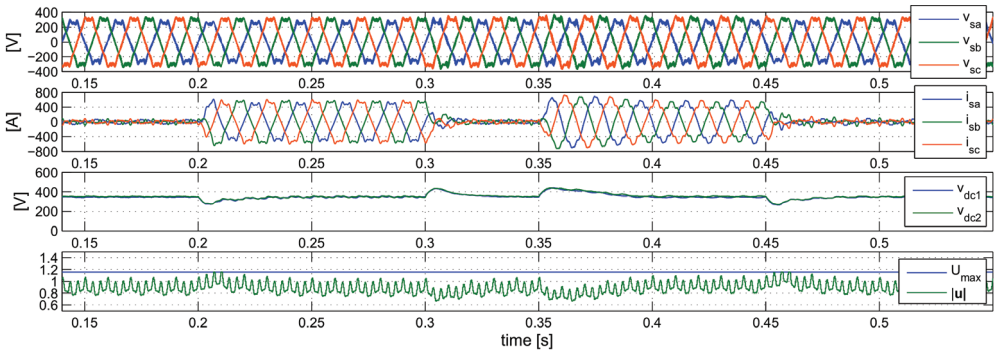

Fig. 6. Performance of the control system – LQ current controller without oscillatory terms

In the first case, the designed current controller is applied without oscillatory terms, wherein the grid voltage, grid currents, DC-link voltages and module of control vector are presented in Fig. 6. The control signal amplitudes are limited in transient states. However, lack of the oscillatory terms results in unbalanced and distorted grid currents. In the second case, the LQ current controller with oscillatory terms and without the developed active damping mechanism is used.

To illustrate the reason why the control signals go beyond the permissible limit, the components of the control signal from individual oscillatory terms are presented in *dq* reference frame. As shown in Fig. 7, the control vector module exceeds the above $U_{\max}$ limit, when SMES charging is started or when SMES discharging is rapidly stopped, which may lead to unsafe operation of the grid-side converter. In these cases, this overrun takes place due to the transient amplitude increase of the u_d^6 and u_d^{12} signals. In the steady-state, the oscillatory terms are mainly stimulated by appropriate higher harmonics in the tracking error of the current loop which are

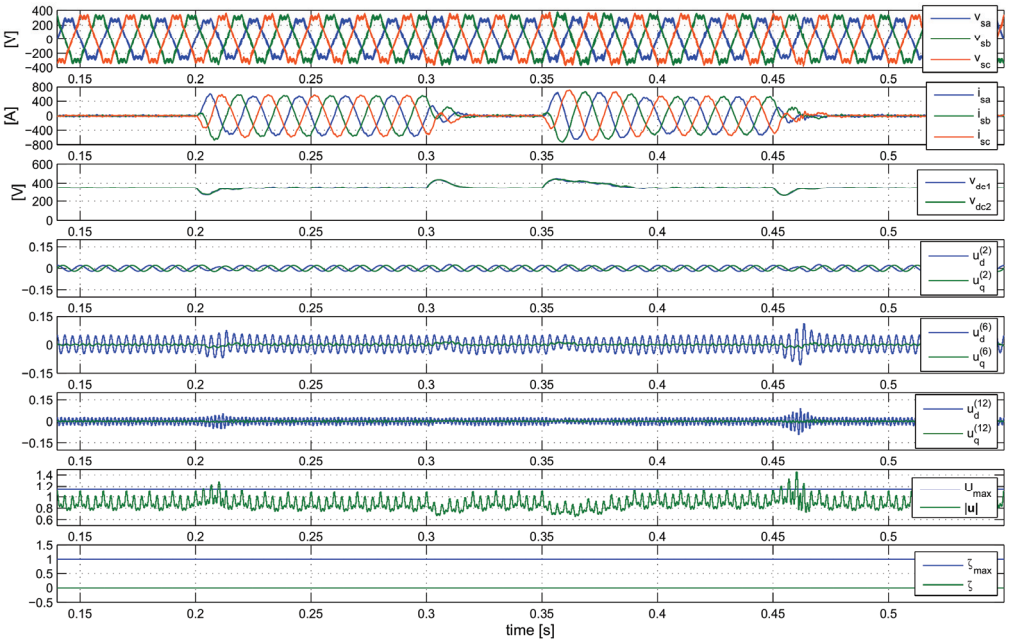

Fig. 7. Performance of the LQ current control system with oscillatory terms and without active damping mechanism, under distorted grid voltage condition

related to the grid voltage disturbances. However, in dynamic states, associated with grid-tie VSC load variation, the i_d^{ref} signal changes abruptly introducing

a wide spectrum of higher harmonic to the tracking error signals in the current loop. Depending on the type of the disturbances occurring suddenly, the resultant level of the individual higher harmonics in the e_d and e_q signals can rapidly increase or decrease, which strongly influences the response of the oscillatory terms. As presented in Fig. 9, the exceeding of the $U_{\max}$ limit by $|\mathbf{u}|$ occurs for a short period of time when grid-tie converter operates in the current limit caused by grid voltage dip.

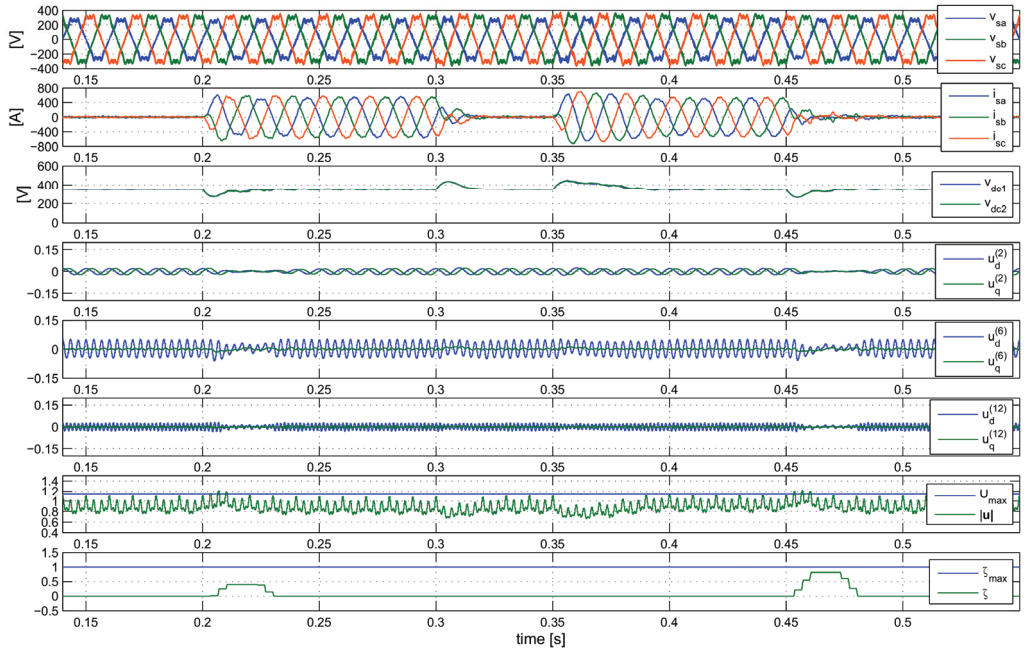

Fig. 8. Performance of the LQ current control system with oscillatory terms and with active damping mechanism, under distorted grid voltage condition

In the third case, the LQ controller with actively damped oscillatory terms is applied. As presented in Fig. 8, the damping factor is increased significantly in the dynamic states resulting in almost complete suppression of oscillatory terms limiting their influence on the control signals. Similarly, in Fig. 10 the damping factor is increased to 0.2 causing a sufficient reduction of oscillatory components in the control signals. Accordingly, the grid current unbalance increases and corresponds to the grid voltage shape.

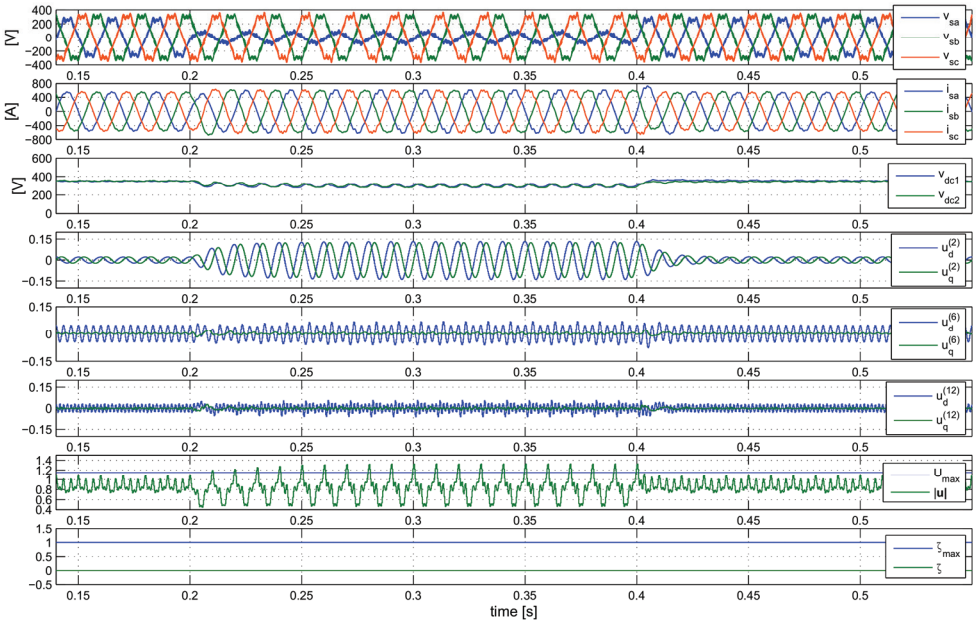

Fig. 9. Performance of the LQ current control system with oscillatory terms and without active damping mechanism, under voltage dip

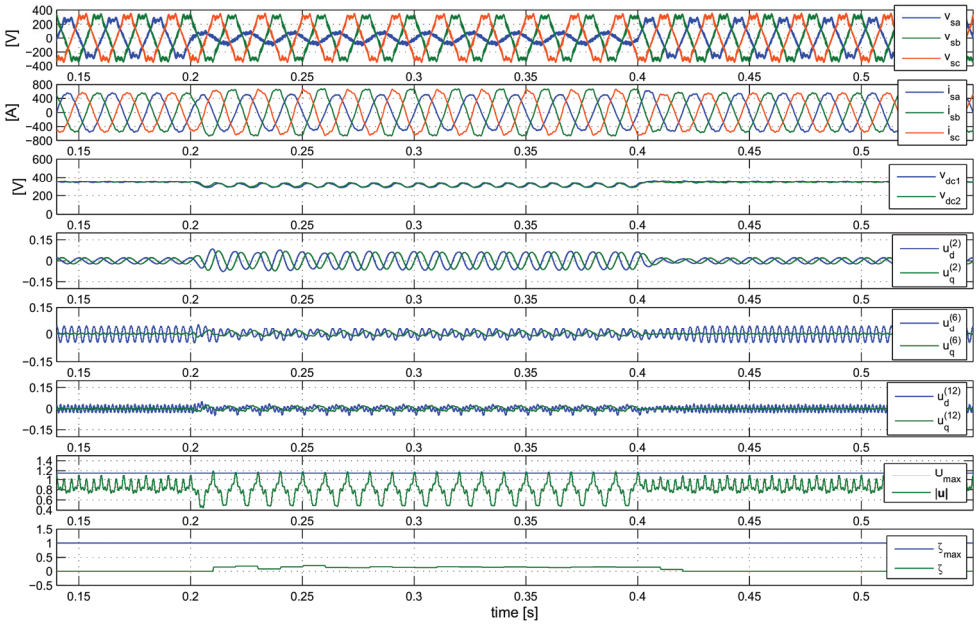

Fig. 10. Performance of the LQ current control system with oscillatory terms and without active damping mechanism, under voltage dip

As presented in Fig. 10, the grid currents are more disturbed than the corresponding ones in Fig. 9 in the time interval from 0.2 s to 0.4 s. In Fig. 9, when active damping mechanism is disabled, the current is closer to sinusoidal, but $|\mathbf{u}|$ is exceeding the $U_{\max}$ limit and unwanted overmodulation occurs. If the active damping mechanism is enabled, the oscillatory terms are actively damped and the tracking error of the current loop cannot be reduced to the level corresponding to the achieved current shape in Fig. 10. However, the unwanted overmodulation is ousted, which is a priority.

5. SUMMARY

An anti-windup strategy for LQ current control with oscillatory terms dedicated to grid-tie VSC in SMES systems has been developed. In order to obtain nearly symmetrical shape of the grid current, the selected damped oscillatory terms linked with most influential low-order harmonics are introduced. As numerical results demonstrate the use of novel SMA-based method of adjusting the damping in oscillatory terms effectively contributes the to reduction of exceeding the control signals beyond the accepted level. The anti-windup mechanism developed works quickly in dynamic states associated with VSC load variation and softly in the case of grid voltage sags, when the converter is in the current limit. Active damping mechanism gives the ability to increase the current feedback gain without overshot caused by temporarily exaggerated feedback from undamped oscillatory terms.

ACKNOWLEDGMENTS

The research was supported by the National Centre for Research and Development (Narodowe Centrum Badań i Rozwoju) within the project No. PBS3/A4/13/2015 entitled "Superconducting magnetic energy storage with a power electronic interface for the electric power systems" (original title: *Nadprzewodzący magazyn energii z interfejsem energoelektronicznym do zastosowań w sieciach dystrybucyjnych*), 01.07.2015–30.06.2018.

REFERENCES

[1] JÍLEK R., GURECKÝ J., RUSNOK S., SOBOTA P., *Electricity storage systems using compressed air*, 16th International Scientific Conference on Electric Power Engineering EPE'2015, Switzerland, 2015, 453–458.

[2] SAEZ-DE-IBARRA A., MARTINEZ-LASERNA E., STROE D., ŚWIERCZYŃSKI M., RODRIGUEZ P., *Sizing Study of Second Life Li-ion Batteries for Enhancing Renewable Energy Grid Integration*, IEEE Transactions on Industry Applications, 2016, 52, 6, 4999–5008.

[3] AWADALLAH M.A., VENKATESH B., *Energy Storage in Flywheels: An Overview*, Canadian Journal of Electrical and Computer Engineering, 2015, 38, 2, 183–193.

[4] ALI M.H., WU B., DOUGAL R.A., *An Overview of SMES Applications in Power and Energy Systems*, IEEE Transactions on Sustainable Energy, 2010, 1, 1, 38–47.

[5] ORŁOWSKA-KOWALSKA T., BLAABJERG F., RODRÍGUEZ J., *Advanced and Intelligent Control in Power Electronics and Drives*, Springer, 2014.
[6] SHAYESTEHFARD A., MEKHILEF S., MOKHLIS H., *IZDPWM-Based Feedforward Controller for Grid-Connected Inverters under unbalanced and distorted conditions*, IEEE Trans. on Industrial Electronics, 2016, 99, 1–1.
[7] HAMOUDA M., BLANCHETTE H.F., AL-HADDAD K., *Unity Power Factor Operation of Indirect Matrix Converter Tied to Unbalanced Grid*, IEEE Transactions on Power Electronics, 2016, 31, 2, 1095–1107.
[8] BUCCELLA C., KHALID H.A., CECATI C., XU D., *On flatness-based controller for shuntconnected VSC with LCL-filter for voltage dip mitigation in a weak grid*, 41st Annual Conference of the IEEE IECON'2015, Japan, 2015.
[9] JUDEWICZ M.G., GONZÁLEZ S.A., ECHEVERRÍA N.I., FISCHER J.R., CARRICA D.O., *Generalized Predictive Current Control for Grid-Tie Three-Phase Inv.*, IEEE Trans. on Industr. Electronics, 2016, 63, 7, 4475–4484.
[10] KAZMIERKOWSKI M., JASIŃSKI M., WRONA G., *DSP-Based Control of Grid-Connected Power Converters Operating Under Grid Distortions*, IEEE Transaction on Industrial Informatics, 2011, 7, 2, 204–211.
[11] DANNEHL J., FUCHS F., THOGERSEN P., *PI State Space Current Control of Grid-Connected PWM Converters With LCL Filters*, IEEE Trans. on Power Electr., 2010, 25, 9, 2320–2330.
[12] YANG Y., ZHOU K., BLAABJERG F., *Enhancing the Frequency Adaptability of Periodic Current Controllers With a Fixed Sampling Rate for Grid-Conn. Power Conv.*, IEEE Trans. on Power Electr., 2016, 31, 10, 7273–7285.
[13] PENG Y., VARANCIC D., HANUS R., WELLER S., *Anti-Windup Designs for Multivariable Controllers*, Automatica, 1998, 34, 12, 1559–1565.
[14] RICHTER S.A., DONCKER R.W.D., *Digital PR control with anti-windup applied to a voltage source inverter*, Power, Proc. of the 2011, 14th European Conf. on Electronics and Applications (EPE 2011), 2011, 1–10.
[15] BOTTRELL N., GREEN T.C., *Comparison of Current-Limiting Strategies During Fault RideThrough of Inverters to Prevent Latch-Up and Wind-Up*, IEEE Transactions on Power Electronics, 2014, 29, 7, 3786–3797.
[16] SZYPULSKI M., IWAŃSKI G., *Sensorless State Control of Stand-Alone Doubly Fed Induction Generator Supplying Nonlinear and Unbalanced Loads*, IEEE Transactions on Energy Conversion, 2016, PP, 99, 1–1.
[17] HARNEFORS L., YEPES A.G., VIDAL A., DOVAL-GANDOY J., *Multifrequency Current Control With Distortion-Free Saturation*, IEEE Journal of Emerging and Selected Topics in Power Electronics, 2016, 4, 1, 37–43.
[18] BUSADA C.A., JORGE S.G., LEON A.E., SOLSONA J.A., *Current Controller Based on Reduced Order Generalized Integrators for DGS*, IEEE Transactions on Industrial Electronics, 2012, 59, 7, 2898–2909.
[19] SMITH S.W., *Digital Signal Processing: A Practical Guide for Engineers and Scientists*, California Technical Publishing, 2002.
[20] DOS SANTOS E.C., CABRAL DA SILVA E.R., In: *Neutral-Point-Clamped Configuration, in Advanced Power Electronics Converters: PWM Converters Processing AC Voltages*, John Wiley and Sons, 2014.
[21] BERES R., WANG X., BLAABJERG F., BAK C.L., LISERRE M., *A review of passive filters for grid-connected voltage source converters*, IEEE Applied Power Electronics Conf. and Exposition (APEC'2014), China 2014, 2208–2215.
[22] LINN Z., KAKIGANO H., MIURA Y., ISE T., *Comparison of power converter circuits for HVDC with SMES*, 14th European Conference on Power Electronics and Applications (EPE'2011), United Kingdom, 2011, 1–10.

[23] INDU P.S., JAYAN M. V., *Frequency regulation of an isolated hybrid power system with Superconducting Magnetic Energy Storage*, 2015 International Conf. on Power, Instrum., Control and Computing (PICC'2015), India, 2015, 1–6.
[24] *Control system of the grid-connected converter based on a state current regulator with oscillatory terms*, Przegląd Elektrotechniczny (Electrical Review), 2015, 91, 1, 65–69.
[25] HODEL A.S., HALL C.E., *Variable-structure PID control to prevent integrator windup*, IEEE Trans. on Ind. Electronics, 2001, 48, 2, 442–451.
[26] NASLIN P., *Essentials of optimal control*, 1968.
[27] GAŁECKI A., KASZEWSKI A., UFNALSKI B., GRZESIAK L.M., *State current controller with oscillatory terms for three-level grid-connected PWM rectifiers under distorted grid voltage conditions*, 17th European Conf. on Power Electronics and Appl. (EPE 2015), Switzerland, 2015.
[28] WANG Y.F., LI Y.W., *Grid Synchronization PLL Based on Cascaded Delayed Signal Cancellation*, IEEE Transactions on Power Electronics, 2011, 26, 7, 1987–1997.
[29] FRANKLIN G.F., POWELL J.D., EMAMI-NAEINI A., In: *Feedback Control of Dynamic Systems* (7th Edition),Chapter 7.5.2, Pearson, 2014.
[30] SALIM R., KANAAN H., AL-HADDAD K., KHEDJAR B., *LQR with integral action controller applied to a three-phase three-switch three-level AC/DC converter*, 36th Annual Conference on Industrial Electronics Society IECON'2010, USA, 2010, 550–555.
[31] KEDJAR B., KANAAN H.Y., AL-HADDAD K., *Vienna Rectifier With Power Quality Added Function*, IEEE Transactions on Industrial Electronics, 2014, 61, 8, 3847–3856.
[32] GAŁECKI A., KASZEWSKI A., UFNALSKI B., GRZESIAK L.M., *LQ current control for three-phase PWM rectifiers under unbalanced grid voltage conditions*, 9th International Conference on Compatibility and Power Electronics (CPE'2015), Portugal, 2015, 191–196.
[33] UFNALSKI B., KASZEWSKI A., GRZESIAK L.M., *Particle Swarm Optimization of the Multioscillatory LQR for a Three-Phase Four-Wire Voltage-Source Inverter With an LC Output Filter*, IEEE Transactions on Industrial Electronics, 2015.